



This is the accepted manuscript made available via CHORUS. The article has been published as:

Analyzing the effect of cell rearrangement on Delta-Notch pattern formation

Toshiki Oguma, Hisako Takigawa-Imamura, Tomoyasu Shinoda, Shuntaro Ogura, Akiyoshi Uemura, Takaki Miyata, Philip K. Maini, and Takashi Miura

Phys. Rev. E **107**, 064404 — Published 14 June 2023

DOI: [10.1103/PhysRevE.107.064404](https://doi.org/10.1103/PhysRevE.107.064404)

Abstract

11

12 The Delta-Notch system plays a vital role in many areas of biology and typically forms a salt
13 and pepper pattern in which cells strongly expressing Delta and cells strongly expressing Notch
14 are alternately aligned via lateral inhibition. In this study, we consider cell rearrangement events,
15 such as cell mixing and proliferation, that alter the spatial structure itself and affect the pattern
16 dynamics. We model cell rearrangement events by a Poisson process and analyze the model while
17 preserving the discrete properties of the spatial structure. We investigate the effects of the inter-
18 mittent perturbations arising from these cell rearrangement events on the discrete spatial structure
19 itself in the context of pattern formation and by using an analytical approach, coupled with nu-
20 merical simulation. We find that the homogeneous expression pattern is stabilized if the frequency
21 of cell rearrangement events is sufficiently large. We analytically obtain the balanced frequencies of
22 the cell rearrangement events where the decrease of the pattern amplitude, as a result of cell rear-
23 rangement, is balanced by the increase in amplitude due to the Delta-Notch interaction dynamics.
24 ~~Our theoretical results are qualitatively consistent with experimental results, supporting the notion~~
25 ~~that the heterogeneity of expression patterns is inversely correlated with cell rearrangement *in vivo*.~~
26 Our framework, while applied here to the specific case of the Delta-Notch system, is applicable
27 more widely to other pattern formation mechanisms.

28 I. INTRODUCTION

29 Discrete cell models can provide different pattern dynamics to those arising from contin-
30 uous cell density models. Because living tissue is made up of cells, which act as the smallest
31 discrete units in space, pattern formation on discrete spatial structures is observed in the
32 context of biological pattern formation on a cellular scale. We study the effects of typical
33 perturbations on the discrete spatial structure itself - flipping and duplication of the lattice
34 - on pattern dynamics using analytical methods.

35 As a mechanism that generates periodic pattern on a cellular scale, we will consider
36 the Delta-Notch system. The Delta-Notch system is a well-studied cell-cell communication
37 system and plays a critical role in many developmental processes [1–15]. Delta and Notch
38 are, respectively, cell surface ligands and receptors. Delta expression in the neighborhood of
39 a cell increases Notch expression in that cell which, in turn, decreases its Delta expression -

40 a process known as “lateral inhibition”. As a result, cells strongly expressing Delta and cells
41 strongly expressing Notch are aligned alternately (the so-called, “salt and pepper” pattern)
42 [5].

43 Collier *et al.* [2] constructed the first mathematical model for the Delta-Notch system,
44 which consisted of a spatially discrete ordinary differential equation system which was then
45 analyzed, and necessary and sufficient conditions for a salt and pepper pattern were derived.
46 To account for stochasticity in the cell-cell interactions and gene expression in signal trans-
47 duction [16–18], a number of subsequent theoretical studies have incorporated stochasticity
48 and revealed that, while low-intensity noise contributes to fine-grained pattern formation,
49 high-intensity noise disrupts the salt and pepper pattern [16, 19, 20].

50 However, little research has been conducted to investigate the effect of positional pertur-
51 bations arising from cell mixing and proliferation, despite these phenomena being generally
52 observed [21–25]. Therefore, cell rearrangement by cell mixing and proliferation should sig-
53 nificantly affect Delta-Notch pattern formation since the cells of interacting neighbors are
54 changing. Germano *et al.* have used a computational model to show that excessive cell
55 turnover homogenizes Delta expression [26], while Stepanova *et al.*[27] developed a com-
56 putational model to investigate how vascular structures are rearranged in response to the
57 VEGF-Delta-Notch system. However, to analytically understand the effect of cell rearrange-
58 ment on pattern formation, a simpler model is required.

59 In this study, we provide a framework to analytically evaluate the effect of stochastic
60 and spatial perturbations arising from cell mixing and proliferation. We construct a simple
61 stochastic differential equation model that incorporates Delta-Notch interaction and cell
62 rearrangement events (cell mixing and proliferation) in one spatial dimension. Our numerical
63 simulations show that the effect of cell rearrangement is to stabilize the homogeneous steady
64 state, and we provide a framework to analytically evaluate the stability of the pattern
65 dynamics. Our analytical framework is consistent with numerical calculations, and provides
66 insight into how model parameters and frequencies of flipping or proliferation balance in the
67 context of pattern formation. ~~Furthermore, we experimentally confirm our ideas through~~
68 ~~observations of the murine retinal vasculature.~~

69 II. METHODS AND MODELS

70 A. Numerical simulations

71 The numerical simulations were performed using Mathematica (Wolfram) and Julia
72 (MIT), and we used periodic boundary conditions and an explicit Euler scheme.

73 For simulation of the Collier model (1), we used the following conditions, unless otherwise
74 stated in the figure captions. Initial cell number $n = 100$, time step $\Delta t = 0.001$, duration $t =$
75 1000 (iteration 1000000), and parameter set $(v, \beta, h, r) = (1, 100, 4, 40)$. Initial conditions
76 are $D_x(0) = D^0 + \kappa$ and $N_x(0) = N^0 + \kappa$. Here D^0 and N^0 are the spatially homogeneous
77 steady state values (Appendix A), and κ is an independent random variable from the uniform
78 distribution in $[-0.0001, 0.0001]$.

79 To incorporate cell flipping and proliferation in the Delta-Notch model (1), we assumed
80 that these events occur following a Poisson process with rates p and q , respectively.

81 B. Classical Delta-Notch model

82 To model the effect of cell mixing or proliferation on Delta-Notch pattern formation, we
83 started with a version of the Collier model [2]. In this model, the Delta and Notch activities
84 of a cell x (D_x and N_x , respectively) in a one-dimensional cell line were modeled (Fig. 1(A))
85 as below:

$$\begin{aligned} \frac{dD_x}{dt} &= v \left(\frac{1}{1 + \beta N_x^h} - D_x \right) \\ \frac{dN_x}{dt} &= \frac{r (D_{x-1} + D_{x+1})}{1 + r (D_{x-1} + D_{x+1})} - N_x. \end{aligned} \quad (1)$$

86 Here, the parameter v denotes the reaction speed of Delta dynamics relative to that of Notch.
87 The parameters h and β denote the Hill coefficient and the intensity of Delta suppression by
88 Notch, respectively. As the Delta activity in neighboring cells ($D_{x-1} + D_{x+1}$) increases, the
89 activation of the Notch activity also increases, reaching a saturation level. The parameter r
90 is a measure of the intensity of Notch activation by the Delta presented in neighboring cells.
91 The number of cells is n and the position of the cell is x ($x \in \mathbb{N}, 1 \leq x \leq n$).

92 We used a one-dimensional model because it is tractable analytically, and the distinct
93 salt and pepper pattern of Delta-Notch expression has been reported in endothelial cells

94 which are aligned one-dimensionally [8, 13, 14]. We assume that the number of cells is
 95 sufficiently large so that we can use periodic boundary conditions. This is because the effect
 96 of boundary conditions is confined near the boundary, and the global pattern we focused
 97 on is minimally affected by the precise form of the boundary conditions if the system size
 98 is large. We confirmed, using numerical simulation, that the main results of this study are
 99 robust to different imposed boundary conditions (results not shown).

100 In the Collier model we use (1), whether or not a salt and pepper pattern emerges depends
 101 on the model parameters (v, β, h, r) . The necessary and sufficient conditions for salt and
 102 pepper pattern formation are obtained by performing a standard linear stability analysis
 103 (Appendix A), requiring that the maximum eigenvalue be greater than zero:

$$\lambda_{\max} = \frac{-(a+d) + \sqrt{(a+d)^2 - 4(ad - 2b\alpha)}}{2} > 0, \quad (2)$$

104 where $a = v$, $b = (\beta hv(N^0)^{h-1}) / (1 + \beta(N^0)^h)^2$, $d = 1$, $\alpha = r / ((1 + 2rD^0)^2)$ and (D^0, N^0)
 105 is the spatially homogeneous steady state of the Collier model (1). For example, the pa-
 106 rameter β , which indicates the intensity of Delta suppression by Notch, broadens the region
 107 where $\lambda(\theta)$ is positive and increases λ_{\max} (Appendix A and Fig. S1 [28]). Based on this
 108 analysis, we proceeded to investigate how pattern formation is altered by cell mixing and
 109 proliferation.

110 C. Cell mixing model

111 To introduce the effect of cell mixing on the Collier model (1), we modeled cell mixing as a
 112 series of flips between neighboring cells. We made several assumptions as follows (Fig. 1(B)):

113 (M1) The positions of the neighboring cells are randomly exchanged by cell flips in a single
 114 step.

115 (M2) Flips occur according to a Poisson process with intensity p in each pair of the cells.

116 Let the vertical vectors \mathbf{D} and \mathbf{N} , respectively, denote Delta and Notch expression in
 117 each cell as below:

$$\begin{aligned} \mathbf{D} &= (D_1, D_2, \dots, D_x, \dots, D_n)^\top \\ \mathbf{N} &= (N_1, N_2, \dots, N_x, \dots, N_n)^\top, \end{aligned} \quad (3)$$

118 and a flip between cells $x = j$ and $x = j + 1$ is described by multiplication with the $n \times n$
 119 matrix A^j , which is generated by swapping the j -th and $j + 1$ -th rows of the identity matrix
 120 as below:

$$\{A^j\}_{k,m} = \begin{cases} 1 & \text{if } (k = m \text{ and } k \neq j, j + 1) \\ & \text{or } (k = j \text{ and } m = j + 1) \\ & \text{or } (k = j + 1 \text{ and } m = j) \\ 0 & \text{otherwise} \end{cases}, \quad (4)$$

121 where $j + 1$ is regarded as 1 if $j = n$ (periodic boundary condition). The effect of cell flipping
 122 was introduced by stochastically multiplying the matrix A^j by \mathbf{D} and \mathbf{N} . Hence, our cell
 123 mixing model is defined by the system of stochastic differential equations as below:

$$\begin{aligned} d\mathbf{D} &= \mathbf{f}(\mathbf{D}, \mathbf{N})dt + \sum_{j=1}^n (A^j - I) \mathbf{D} dL_t^{p,j} \\ d\mathbf{N} &= \mathbf{g}(\mathbf{D}, \mathbf{N})dt + \sum_{j=1}^n (A^j - I) \mathbf{N} dL_t^{p,j}, \end{aligned} \quad (5)$$

124 where the functions \mathbf{f} and \mathbf{g} are the reaction terms of the Collier model (1), the matrix I de-
 125 notes the identity matrix and $L_t^{p,j}$ is the Poisson process with intensity p , which corresponds
 126 to the flip between cells j and $j + 1$.

127 **D. Cell proliferation model**

128 To introduce the effect of cell proliferation on the Collier model (1), we modeled cell
 129 proliferation as the duplication of a cell. We also made several assumptions as follows
 130 (Fig. 1(C)):

131 (P1) The duplication process occurs in a single step.

132 (P2) The new cell is placed to the right of the original cell and inherits the same levels of
 133 Delta and Notch of the original cell.

134 (P3) The duplication process occurs according to the Poisson process with intensity q in
 135 each cell.

136 Assumptions (P2) and (P3) implicitly assume, respectively, that Delta and Notch activities
 137 are determined by their concentrations [29], and cell proliferation follows a memoryless

138 stochastic process [30]. We denote Delta and Notch expression by the vertical vectors $\mathbf{D}_n =$
 139 $(D_1, D_2, \dots, D_n)^\top$ and $\mathbf{N}_n = (N_1, N_2, \dots, N_n)^\top$, respectively. Note that the number of cells
 140 (the dimension of the vectors \mathbf{D}_n and \mathbf{N}_n) n increases with time. Under these assumptions,
 141 duplication of cell j is accounted for by defining the $(n+1) \times n$ matrix B^j , which is generated
 142 by duplicating the j -th row of the identity matrix as below:

$$\{B^j\}_{k,m} = \begin{cases} 1 & \text{if } (k = m \text{ and } k \leq j) \\ & \text{or } (k = m + 1 \text{ and } k \geq j), \\ 0 & \text{otherwise} \end{cases}, \quad (6)$$

143 and stochastically multiplying this matrix by \mathbf{D}_n and \mathbf{N}_n , respectively:

$$\begin{aligned} \text{If } dL_t^{q,j} = 0, & \begin{cases} \mathbf{D}_n(t+dt) = \mathbf{D}_n(t) + \mathbf{f}(\mathbf{D}_n, \mathbf{N}_n)dt \\ \mathbf{N}_n(t+dt) = \mathbf{N}_n(t) + \mathbf{g}(\mathbf{D}_n, \mathbf{N}_n)dt \end{cases} \\ \text{If } dL_t^{q,j} = 1, & \begin{cases} \mathbf{D}_{n+1}(t+dt) = B^j [\mathbf{D}_n(t) + \mathbf{f}(\mathbf{D}_n, \mathbf{N}_n)dt] \\ \mathbf{N}_{n+1}(t+dt) = B^j [\mathbf{N}_n(t) + \mathbf{g}(\mathbf{D}_n, \mathbf{N}_n)dt] \end{cases} \end{aligned} \quad (7)$$

144 Note that n will increase with time according to the Poisson process, so the size of B^j will
 145 also increase with time.

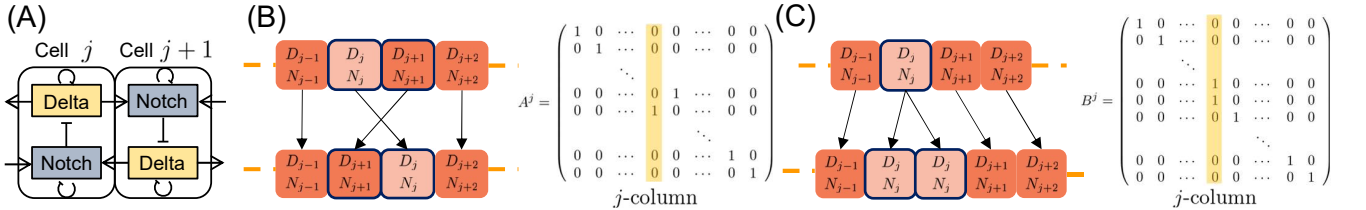


FIG. 1. (A) Schematic of the Delta-Notch interaction in the Collier model. Notch expression inhibits Delta expression, Delta expression promotes Notch expression in adjacent cells, and Delta and Notch themselves naturally decay. (B) Schematic of the flip event in the cell mixing model and the matrix A^j in (4). The flip event occurs according to the Poisson process with intensity p in each pair of cells. (C) Schematic of the duplication event in the cell proliferation model and the matrix B^j in (6). The duplication event occurs according to the Poisson process with intensity q in each cell.

146 III. RESULTS

147 A. Numerical simulations with cell rearrangement

148 We set the parameters (v, β, h, r) such that linear analysis predicts the salt and pepper
149 pattern when there is no cell rearrangement (without cell mixing or proliferation) and we
150 simulated the model (Fig. 2(A)). We then included cell rearrangement and found that the
151 heterogeneity of the Delta-Notch pattern was decreased by cell rearrangement, and the ho-
152 mogeneous steady state became stable again for a sufficiently high level of cell rearrangement
153 (Fig. 2(B)). More precisely, when the flip frequency $p = 0.001$, the salt and pepper pattern
154 was largely maintained. However, for increasing values of p , the amplitude of the pattern
155 became smaller. When p was sufficiently large, the amplitude was almost 0 for the whole
156 region, and the system relaxed to the spatially homogeneous steady state (Fig. 2(B)). In
157 addition, as p increases, the expression pattern shows an envelope structure, in which the
158 amplitude of the periodic pattern follows a longer pattern that oscillates. Similar results
159 were obtained with the cell proliferation model (Fig. 2(C)). With increasing proliferation
160 frequency q , the amplitude of the pattern became smaller and, finally, the system settled
161 back to a homogeneous steady state. These results are robust to 100 different runs of nu-
162 merical simulations for each parameter set. Corresponding results are also obtained with
163 different values of β and r (Fig. S2 and Fig. S3 [28]), suggesting that the stabilization of the
164 homogeneous steady state by cell rearrangement events is a robust phenomenon.

165 To quantify the heterogeneity of the expression pattern, we introduce the heterogeneity
166 function, $H(t)$, as the variance of the Delta expression:

$$H(t) = \frac{1}{n} \sum_{x=1}^n [D_x(t)^2 - \langle D(t) \rangle^2], \quad (8)$$

167 where

$$\langle D(t) \rangle = \frac{1}{n} \sum_{x=1}^n D_x(t). \quad (9)$$

168 If the salt and pepper pattern is completely formed, then $H(t)$ is close to the squared value
169 of the amplitude of the pattern. If Delta expression is spatially homogeneous at the steady
170 state, then $H(t) = 0$.

171 In both models, at the onset of the simulation, $H(t)$ decreases and then either increases
172 or still decreases depending on the value of p in the cell mixing model or the value of q in

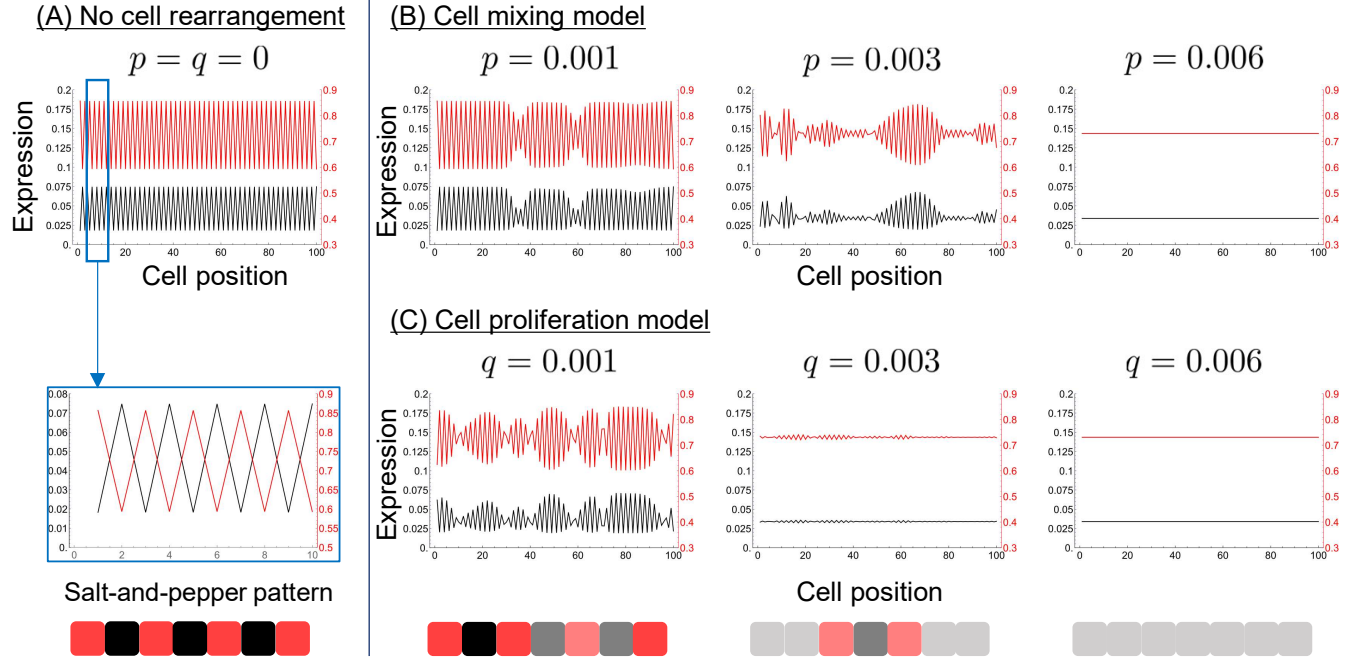


FIG. 2. Numerical simulations of the standard Delta-Notch model (1), the cell mixing model (5) and the cell proliferation model (7). (A) Standard model (no cell rearrangement). The red line represents Notch expression and the black line represents Delta expression. Delta and Notch are alternately expressed, and the classical salt and pepper pattern emerges. (B) Cell mixing model (5). Numerical simulations are performed for different flipping frequencies $p = 0.001, 0.003, 0.006$. (C) Cell proliferation model (7). Numerical simulations are performed for different proliferation frequencies $q = 0.001, 0.003, 0.006$. The expression patterns of the first 100 cells are shown. Initial cell number $n = 100$, time step $\Delta t = 0.01$, duration $t = 1000$, and $(v, \beta, h, r) = (1, 100, 4, 40)$. Initial condition, $D_x(0) = D^0 + \kappa_x$ and $N_x(0) = N^0 + \kappa_x$, where D^0 and N^0 are the spatially homogeneous steady state values (Appendix A), and κ_x is a random variable from the uniform distribution in $[-0.02, 0.02]$.

173 the cell proliferation model (Figs. S4 and S5 [28]). This is because, at the onset, the initial
 174 random state is smoothed by the Delta-Notch dynamics. As we are interested in pattern
 175 growth after a sufficient time has elapsed, we define H_0 as the minimum heterogeneity in
 176 the time evolution of the no cell rearrangement model (Fig. S4 and Table. S1 [28]);

$$H_0 = \text{Min}(H(t)). \quad (10)$$

177 Then we define the normalized heterogeneity $H^*(t)$ as $H^*(t) = H(t)/H_0$, which is plotted

178 in Fig. 3. Figure 3 shows that $H^*(t)$ switches between increasing and decreasing depending
 179 on the values of p and q . In the cell mixing model, it appears that $H^*(t)$ increases for
 180 $p \leq 0.005$ and decreases for $p > 0.005$ (Fig. 3(A) and Fig. S5(A) [28]). In the cell proliferation
 181 model, $H^*(t)$ increases for $q \leq 0.0045$ and decreases for $q > 0.0045$ (Fig. 3(B) and Fig. S5(B)
 182 [28]). These results suggest that there exist balanced frequencies p^* and q^* for which the
 183 attenuation of the pattern by cell rearrangement and its formation by the Delta-Notch
 184 dynamics are balanced.

185 We numerically estimated the balanced frequencies and the growth rate of the hetero-
 186 geneity.

187 For the balanced frequencies p^* and q^* , we estimated the intersection points of the plot of
 188 $\ln H^*(t)$ as a function of p and q and the plot of $\ln H^*(t) = 0$. We performed linear regression
 189 for the data points whose value of $\log_{10} H^* \in [-8, 4]$ in Fig. 3, and estimated p^* and q^* as
 190 the intersection points of the fitted lines and the function $\ln H^*(t) = 0$ (Figs. 4(C) and 4(F),
 191 black dots). For the growth rate of the heterogeneity, we estimated the slope of the line
 192 that was fitted to the plot of $\ln H^*(t)$ against t . Similarly, we performed linear regression
 193 for the data points in the range $\log_{10} H^* \in [-8, 4]$ in Fig. S5 [28], and estimated y and j as
 194 the slopes of the fitted lines (Figs. 4(A) and 4(D), black dots).

195 B. Analysis of the cell rearrangement models

196 To quantify the effects of cell rearrangement (mixing and proliferation), we analyzed
 197 the stability of the pattern dynamics and the balanced frequencies p^* and q^* . The “tug-
 198 of-war” of the cell rearrangement and the Delta-Notch dynamics was represented as the
 199 growth or attenuation of the heterogeneity $H(t)$. Therefore, we focused on the effect of cell
 200 rearrangement on $H(t)$.

201 The heterogeneity $H(t)$ can also be calculated from the power spectrum of the Delta
 202 expression pattern. The power spectrum P_k of the Delta expression pattern are the squared
 203 absolute values of the Fourier coefficients δ_k of Delta expression (Appendix A), so P_k can be
 204 calculated as:

$$P_k(t) = |\delta_k(t)|^2 = \left| \frac{1}{n} \sum_{x=1}^n D_x(t) e^{\frac{-i2\pi kx}{n}} \right|^2. \quad (11)$$

205 Note that k takes integer values from 0 to $n - 1$, and n increases with time in the cell

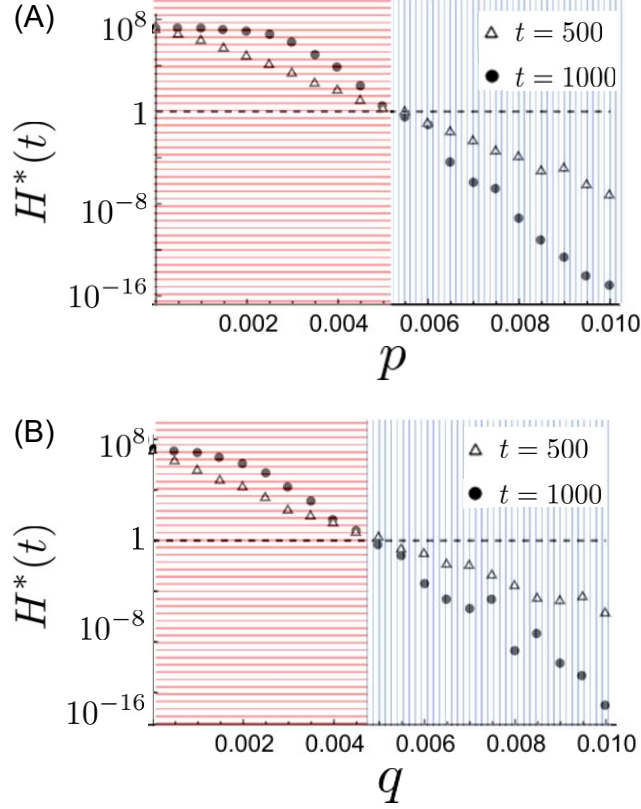


FIG. 3. Log plots of the normalized heterogeneity of the pattern $H^*(t)$ against the frequencies of the cell rearrangement events for $t = 500$ and 1000. The black dashed line represents the plot of $H^*(t) = 1$ and the circles and triangles represent $H^*(1000)$ and $H^*(500)$, respectively. (A) In the cell mixing model, $H^*(1000) > H^*(500) > 1$ with $p \leq 0.005$ (red horizontal stripe region) and $H^*(1000) < H^*(500) < 1$ with $p > 0.005$ (blue vertical stripe region). (B) In the cell proliferation model, similar inequalities hold, and the threshold value is $q = 0.0045$. We calculated the heterogeneity at 21 different frequencies of p and q , which are taken in the range 0 to 0.01 at equal intervals of 0.0005 in each model. The heterogeneity $H^*(t)$ shown in this figure was calculated by taking the average of $H(t)$ over 400 different simulation runs, and then normalized by H_0 , for each p and q . Other conditions are as in Fig. 2. Initial conditions are randomly determined from the same distribution as in Fig 2 for each of the runs.

206 proliferation model. From Parseval's theorem,

$$\sum_{x=1}^n D_x(t)^2 = \sum_{k=0}^{n-1} P_k(t), \quad (12)$$

207 and from (11),

$$\langle D_x(t) \rangle^2 = \left(\frac{1}{n} \sum_{x=1}^n D_x(t) \right)^2 = P_0(t). \quad (13)$$

208 By substituting (12) and (13) into (8), $H(t)$ was calculated as below:

$$H(t) = \frac{1}{n} \sum_{k=1}^{n-1} P_k(t). \quad (14)$$

209 Therefore, $H(t)$ is equal to the sum of squares of the amplitudes of all wavenumber compo-
210 nents in the pattern.

211 The balanced frequencies p^* and q^* are independent of the definition of the heterogeneity
212 $H(t)$. If we adopted the variance of the Notch expression instead of the Delta expression,
213 then the dispersion relation and the effect of the cell rearrangement events A^j and B^j are
214 the same as for Delta expression, and we obtained the same p^* and q^* as before. In addition,
215 we can obtain the same p^* and q^* values if we defined the heterogeneity by the average of
216 the squared values. For example, if we adopt $[\Sigma(D_x - D_{x+1})^2]/n$ as the heterogeneity, then
217 we obtain the same p^* and q^* since this value is also calculated from the linear summation
218 of the power spectrum (Fig. S6 [28]). We now proceed to analyze the stability of the power
219 spectrum $P_k(t)$ in the cell mixing and proliferation models.

220 1. Cell mixing model

221 First, we will transform the cell mixing model (5) into the corresponding system of
222 stochastic differential equations that represent the time evolution of the Fourier coefficients
223 δ_k . To find the balanced frequency p^* and the onset of pattern formation, we assume
224 that $H(t)$ is small since we set the initial condition to be a small perturbation about the
225 homogeneous steady state, so the reaction terms $\mathbf{f}(\cdot)$ and $\mathbf{g}(\cdot)$ can be regarded as linear
226 operators since $D_x \sim D^0$ and $N_x \sim N^0$. Therefore, the effect of the Delta-Notch dynamics
227 on the Fourier coefficients δ_k of D_x is described by the diagonal matrix Λ from the linear
228 stability analysis (Appendix A) as below:

$$\Lambda = \text{Diag}(\lambda_0, \lambda_1, \dots, \lambda_{n-1}), \quad (15)$$

229 where

$$\lambda_k = \frac{-(a+d) + \sqrt{(a+d)^2 - 4(ad + 2b\alpha \cos(2\pi k/n))}}{2}. \quad (16)$$

230 The effect on the Fourier coefficients δ_k of a cell flip is given by the $n \times n$ matrix C^j :

$$C^j = FA^jF^{-1}, \quad (17)$$

231 where F is the discrete Fourier transform matrix. The components of the matrices F and
232 F^{-1} are given as below:

$$\{F\}_{l,m} = \frac{1}{\sqrt{n}} e^{-i2\pi(l-1)(m-1)/n}, \quad (18)$$

$$\{F^{-1}\}_{l,m} = \frac{1}{\sqrt{n}} e^{i2\pi(l-1)(m-1)/n}. \quad (19)$$

233 Therefore, the time evolution of the Fourier coefficients $\boldsymbol{\delta}$ can be described by:

$$d\boldsymbol{\delta} = \Lambda\boldsymbol{\delta}dt + \sum_{j=1}^n (C^j - I)\boldsymbol{\delta}dL_t^{p,j}, \quad (20)$$

234 where $\boldsymbol{\delta} = (\delta_0(t), \delta_1(t), \dots, \delta_k(t), \dots, \delta_{n-1}(t))^T$.

235 Furthermore, we obtain the expected time evolution of the power spectrum by calculating
236 the average of the effect of the cell flip on the power spectrum for j (Appendix B) as below:

237

$$d\mathbf{P} = 2\text{Re}[\Lambda]\mathbf{P}dt + W\mathbf{P}dL_t^{pn}. \quad (21)$$

238 Here $\mathbf{P} = (P_0(t), P_1(t), \dots, P_k(t), \dots, P_{n-1}(t))^T$, L_t^{pn} is the Poisson process with intensity
239 pn , and the components of the matrix W are given as below:

$$\{W\}_{l,m} = \begin{cases} -\frac{8}{n} \sin^2 \frac{\pi(l-1)}{n} + \left(\frac{4}{n} \sin^2 \frac{\pi(l-1)}{n}\right)^2 & (l = m) \\ \left(\frac{4}{n} \sin \frac{\pi(l-1)}{n} \sin \frac{\pi(m-1)}{n}\right)^2 & (\text{otherwise}). \end{cases} \quad (22)$$

240 Both the average and variance of the Poisson process L_t^{pn} are pnt , so those of L_t^{pn}/n are pt
241 and pt/n , respectively. Therefore, when n is sufficiently large, dL_t^{pn}/n can be approximated
242 by pdt and equation (21) is approximated by:

$$\frac{d}{dt}\mathbf{P} \simeq Y_p\mathbf{P}, \quad (23)$$

243 where

$$Y_p = 2\text{Re}[\Lambda] + pnW. \quad (24)$$

244 Therefore, by using the maximum eigenvalue and the corresponding eigenvector of the matrix
245 Y_p , we can derive the expected pattern dynamics.

246 If y is the maximum eigenvalue of Y_p and $\mathbf{P}^* = (P_0^*, P_1^*, \dots, P_{n-1}^*)^\top$ is the corresponding
 247 eigenvector, then $\mathbf{P} \sim e^{yt} \mathbf{P}^*$ for values of t in a range sufficiently large so that other
 248 eigenvectors no longer affect the power spectrum, but not so large for nonlinear effects to
 249 come into play. The scaling law $H(t) \sim e^{yt}$ also holds since $H(t)$ is a linear summation of
 250 the power spectrum $P_k(t)$. Therefore, the maximum eigenvalue y corresponds to the growth
 251 rate of the heterogeneity $d \ln H(t)/dt$. Figure 4(A) shows that the value of y derived from
 252 equation (23) agrees with the numerically estimated growth rate $d \ln H(t)/dt$, and Fig. 4(B)
 253 shows how the shape of the corresponding eigenvector \mathbf{P}^* depends on p . Note that the effect
 254 of the Delta-Notch interaction $2\text{Re}[\Lambda]$ on P_k is determined by the value of $2\pi k/n$, so we plot
 255 P_k^* against $2\pi k/n$ in Fig. 4(B).

256 To obtain the balanced frequency p^* , we used Newton's method to derive the value of
 257 p such that the maximum eigenvalue of Y_p is 0. The values of p^* obtained in this way
 258 are in very good agreement with the corresponding values estimated from the numerical
 259 simulations of (5) for varying β (Fig. 4(C) and S7 [28]) and r (Fig. S8 [28]). In addition,
 260 the values of y and p^* obtained in Figs. 4(A) and 4(C) are almost identical for $n \geq 100$
 261 (Figs. S9(A) and S9(B) [28]).

262 Furthermore, we obtain the growth rate $d \ln H(t)/dt$ and the balanced frequency p^* as
 263 $n \rightarrow \infty$ as solutions of the integral equations (Supplementary text A [28]). They are also in
 264 very good agreement with the numerically estimated values.

265 We can derive an approximation to the balanced frequency p^* from the linear stability
 266 analysis of the spatially uniform steady state in the deterministic system that is obtained
 267 by regarding the effect of cell mixing as a diffusion process:

$$\begin{aligned} \frac{dD_x}{dt} &= v \left(\frac{1}{1 + \beta N_x^h} - D_x \right) + p(D_{x-1} + D_{x+1} - 2D_x) \\ \frac{dN_x}{dt} &= \frac{r(D_{x-1} + D_{x+1})}{1 + r(D_{x-1} + D_{x+1})} - N_x + p(N_{x-1} + N_{x+1} - 2N_x). \end{aligned} \quad (25)$$

268 System (25) has the same spatially homogeneous steady state as in (1), so we can linearize
 269 the system as in Appendix A, and obtain the Jacobian matrix:

$$\tilde{M}_k = \begin{pmatrix} -a - 4p \sin^2(\pi k/n) & -b \\ 2\alpha \cos(2\pi k/n) & -d - 4p \sin^2(\pi k/n) \end{pmatrix}. \quad (26)$$

270 The eigenvalue $\tilde{\lambda}_k$ with the larger real part, obtained from the matrix \tilde{M}_k , is:

$$\tilde{\lambda}_k = \lambda_k - 4p \sin^2 \frac{\pi k}{n}, \quad (27)$$

271 where λ_k is given by (A9), so the time evolution of the power spectrum can be approximated
 272 by:

$$\frac{d}{dt}P_k = \left(2\text{Re}[\lambda_k] - 8p \sin^2 \frac{\pi k}{n}\right) P_k. \quad (28)$$

273 This equation corresponds to the system that is obtained by ignoring the non-diagonal
 274 components of the matrix Y_p in (23). From (28), the balanced frequency p^* is approximated
 275 as p such that:

$$\text{Max}_{\theta \in [0, 2\pi)} \left[\text{Re}[\lambda(\theta)] - 4p \sin^2 \frac{\theta}{2} \right] = 0. \quad (29)$$

276 When the range of θ for which $\lambda(\theta)$ is positive is sufficiently narrow, the values of P_k ,
 277 except around $k = n/2$, quickly decay. Hence, the non-diagonal components of the matrix
 278 Y_p are ignorable and we can approximate the effect of cell mixing as a diffusion of the Delta
 279 and Notch activities.

280 Figure 4(C) shows that the estimation in equation (29) is a good approximation for
 281 $95 < \beta < 120$. If $\lambda(\theta)$ is positive only in the region that is very close to $\theta = \pi$, then we can
 282 obtain the simpler form of (29):

$$p^* = \lambda_{\max}/4. \quad (30)$$

283 Here λ_{\max} is given by equation (2), and we used the approximation $\sin^2(\theta/2) \simeq 1$ in the
 284 region that is close to $\theta = \pi$. Consistent with (30), λ_{\max} was 0.02 and the balanced frequency
 285 p^* was estimated around 0.005 for the conditions used in Fig. 3.

286 2. Cell proliferation model

287 The cell proliferation model (7) was also analytically transformed into the corresponding
 288 system of stochastic differential equations that represent the time evolution of δ_k . The effect
 289 of a cell proliferation event, which increases the cell number n to $n + 1$, on the Fourier
 290 coefficients δ_n , is given as below:

$$\hat{C}^j = \hat{F} B_j F^{-1}, \quad (31)$$

291 where \hat{F} is a square $(n + 1) \times (n + 1)$ matrix, F^{-1} is the square $(n \times n)$ matrix defined in
 292 (19), and B_j is the $(n + 1) \times n$ matrix given by (6). The matrix \hat{F} is defined by:

$$\left\{ \hat{F} \right\}_{l,m} = \frac{1}{\sqrt{n+1}} e^{-i2\pi(l-1)(m-1)/(n+1)}. \quad (32)$$

293 Therefore, the time evolution of $\boldsymbol{\delta}_n(t)$ is given as below:

$$\begin{cases} \boldsymbol{\delta}_n(t + dt) = e^{\Lambda dt} \boldsymbol{\delta}_n(t) & \text{if } dL_t^{q,j} = 0 \\ \boldsymbol{\delta}_{n+1}(t + dt) = \hat{C}^j e^{\Lambda dt} \boldsymbol{\delta}_n(t) & \text{if } dL_t^{q,j} = 1. \end{cases} \quad (33)$$

294 By calculating the average of the effect of the cell proliferation event for j , the expected
295 time evolution of the power spectrum $\mathbf{P}_n(t)$ is given (Appendix C) by:

$$\begin{cases} \mathbf{P}_n(t + dt) = e^{2\text{Re}[\Lambda]dt} \mathbf{P}_n(t) & \text{if } dL_t^{qn} = 0 \\ \mathbf{P}_{n+1}(t + dt) = S e^{2\text{Re}[\Lambda]dt} \mathbf{P}_n(t) & \text{if } dL_t^{qn} = 1, \end{cases} \quad (34)$$

296 where the components of the matrix S are given by:

$$\{S\}_{l,m} = \begin{cases} (n+1)/n & (\text{if } l = m = 1) \\ \frac{1}{n(n+1)} \frac{\sin^2 \frac{\pi m}{n}}{\sin^2(\frac{\pi l}{n+1} - \frac{\pi m}{n})} & (\text{otherwise}). \end{cases} \quad (35)$$

297 Since the matrix S is non-square, the stability of the homogeneous steady state cannot
298 be determined as in the cell mixing model. Hence we approximate the matrix S by a square
299 matrix, as below.

300 The power spectrum \mathbf{P}_n is represented by the superposition of the cosine waves from
301 the symmetry $P_k = P_{n-k}$. By assuming that the shortest wavelength component of $S\mathbf{P}_n$
302 is negligible, the matrix S is approximated by the square matrix Σ (given below) and the
303 equation (34) is approximated by (Appendix C):

$$d\mathbf{P}_n \simeq 2\text{Re}[\Lambda] \mathbf{P}_n dt + (\Sigma - I) \mathbf{P}_n dL_t^{qn}, \quad (36)$$

304 where I is the identity matrix. When n is even, the components of the matrix Σ are given
305 by:

$$\begin{aligned} \{\Sigma\}_{l,m} = & \frac{2}{n} \sum_{k=2}^{n/2} \cos \frac{2\pi(m-1)(k-1)}{n} \left[\frac{k-1}{n+1} \cos \frac{2\pi(l-1)(k-2)}{n} + \left(1 - \frac{k-1}{n+1}\right) \cos \frac{2\pi(l-1)(k-1)}{n} \right] \\ & + \frac{1}{n} \left(1 + (-1)^{m+k-2} \left(1 - \frac{n}{n+1} \sin^2 \frac{\pi(m-1)}{n} \right) \right), \end{aligned} \quad (37)$$

306 and when n is odd:

$$\begin{aligned} \{\Sigma\}_{l,m} = & \frac{2}{n} \sum_{k=2}^{(n+1)/2} \cos \frac{2\pi(m-1)(k-1)}{n} \left[\frac{k-1}{n+1} \cos \frac{2\pi(l-1)(k-2)}{n} + \left(1 - \frac{k-1}{n+1}\right) \cos \frac{2\pi(l-1)(k-1)}{n} \right] \\ & + \frac{1}{n}. \end{aligned} \quad (38)$$

307 As in the cell mixing model, assuming n is sufficiently large, L_t^{qn}/n is approximated by
 308 qt as in the cell mixing model, so the time evolution of \mathbf{P}_n in (36) is approximated by:

$$\frac{d}{dt}\mathbf{P}_n \simeq J_q\mathbf{P}_n, \quad (39)$$

309 where

$$J_q = 2\text{Re}[\Lambda] + qn(\Sigma - I). \quad (40)$$

310 Therefore, by using the maximum eigenvalue and the corresponding eigenvector of the
 311 matrix J_q , we can approximately derive the expected pattern dynamics.

312 Figure 4(D) shows that the maximum eigenvalue of the matrix J_q is in very good agree-
 313 ment with the numerically estimated growth rate $d \ln H(t)/dt$, and Fig. 4(E) shows how the
 314 shape of the corresponding eigenvector \mathbf{P}_n^* depends on q .

315 To obtain the balanced frequency q^* , we used Newton's method to derive the value of
 316 q such that the maximum eigenvalue of J_q is 0. Figure 4(F) shows that the values of q^*
 317 obtained in this way are in very good agreement with the numerically estimated q^* . The
 318 values obtained in Figs. 4(D) and 4(F) are almost identical for $n \geq 100$ (Fig. S9 [28]),
 319 although the definition of the matrix Σ is different whether n is odd or even.

320 *3. The eigenvalue problems corresponding to (23) and (36) explain the pattern dynamics.*

321 In the above analysis, we have shown that the pattern dynamics of the cell mixing model
 322 and the cell proliferation model can be captured by solving for the maximum eigenvalue
 323 problem of the matrices Y_p (24) and J_q (40), respectively, and yield results that agree well
 324 with our numerical simulations of the full model.

325 First, the maximum eigenvalue of Y_p and J_q capture the growth or attenuation rate of the
 326 heterogeneity of the pattern. Figs. 4(A) and 4(D) show that the exponents are consistent
 327 with the maximum eigenvalue y and j . Therefore, the balanced frequencies p^* and q^* are
 328 derived as the frequencies that make $y = 0$ and $j = 0$, respectively (Figs. 4(C), 4(F) and
 329 Fig. S8).

330 Second, the maximum eigenvalues y and j also explain the time for the pattern to be
 331 established. Figures S10(A) and (C) [28] show that the time required for $H(t)$ to reach a
 332 saturated value extends as p and q increase. Here, we define the characteristic time t^* , as
 333 the time required for $H^*(t)$ to reach $H^*(10000)/e$, and find that the values of yt^* and jt^*

334 for each p and q are within an error margin of 8.2 % and 7.3 %, respectively (Figs. S10(B)
 335 and S10(D) [28]). Therefore, cell mixing and cell proliferation extend the time required for
 336 pattern establishment, as $t^* \sim 1/y$ and $t^* \sim 1/j$, respectively.

337 In addition, the eigenvectors corresponding to y and j , shown in Figs. 4(B) and 4(E),
 338 explain the pattern envelope in Fig. 2. Figure 4 shows that, in the model that includes
 339 only the Delta-Notch interaction, the eigenvector corresponding to the maximum eigenvalue
 340 has non-zero component only for $k = n/2$. On the other hand, in the model that includes
 341 cell mixing and proliferation, the eigenvector takes non-zero values for several wavenum-
 342 bers. When several wavelength components are mixed at a similar scale, the corresponding
 343 envelope pattern structure is generated.

344 Although cell mixing and proliferation similarly affect the pattern dynamics as discussed
 345 above, their individual effects on the power spectrum are qualitatively different. We per-
 346 formed numerical simulations of the model including only one of the processes (cell mixing,
 347 cell proliferation) (without the Delta-Notch interaction) setting the salt and pepper pattern
 348 as the initial state. The results show that cell mixing, unsurprisingly, “scrambles” the pat-
 349 tern and the power spectrum is uniformly distributed, while cell proliferation elongates the
 350 periodic length of the pattern and shifts the power spectrum to the long-wavelength region
 351 (Fig. S11 [28]). This is because both effects are regarded as the redistribution of the power
 352 spectrum in frequency space since the determinants of W and Σ in equations (22) and (37
 353 and 38) are 1. Their eigenvectors, corresponding to the maximum eigenvalues, are shown in
 354 Fig. S11(E) [28]. The components of the eigenvector of W are all equal to each other, and
 355 that of Σ has only one non-zero components for ($k = 0$). These results mean that cell mixing
 356 coarsens the power spectrum so that it becomes uniformly distributed, while cell prolifer-
 357 ation shifts the distribution of the power spectrum to the long-wavelength region. These
 358 difference correspond, in the absence of cell-cell interaction, to the scrambling of existing
 359 patterns due to cell mixing, and elongation of an existing pattern due to cell proliferation.
 360 However, when they are incorporated into the Delta-Notch model, the pattern dynamics
 361 are dominated by the interaction between the increasing power spectrum around $k = n/2$
 362 by Delta-Notch interaction and its redistribution by cell rearrangement, and the pattern
 363 dynamics in cell mixing and proliferation model become similar.

364 Based on the above discussion, the pattern dynamics of the Delta-Notch interaction with
 365 cell rearrangement events results in the growth and redistribution of the power spectrum. In

366 the model that includes only Delta-Notch interaction, the power spectrum around $k = n/2$
 367 grows according to the dispersion-relation, while the rest of the spectrum decays (Appendix
 368 A). As a result, the power spectrum finally concentrates around $k = n/2$, which corresponds
 369 to the salt and pepper pattern. However, when cell mixing and proliferation are introduced,
 370 the power spectrum around $k = n/2$ is distributed to other regions and undergoes attenua-
 371 tion. If the attenuation of the redistributed power spectrum exceeds the growth of the power
 372 spectrum around $k = n/2$, then the sum of the power spectrum decreases, which means that
 373 the homogeneous steady state is stabilized. The cell flip or proliferation frequency at the
 374 balanced point is the balanced frequency p^* and q^* . Note that cell mixing and proliferation
 375 themselves do not stabilize the homogeneous steady state, but require the attenuation of the
 376 redistributed power spectrum due to the Delta-Notch interaction. Therefore, if the Delta and
 377 Notch activities are bistable without spatial interactions, as reported by Formosa-Jordan *et*
 378 *al.* [31], then the redistributed power spectrum is not attenuated. Hence the pattern is not
 379 homogenized, only disturbed.

380 IV. DISCUSSION

381 To our knowledge, this paper is the first to provide a framework to analytically evaluate
 382 the effect on Delta-Notch pattern formation of cell rearrangement arising from migration
 383 or proliferation in a one-dimensional line of cells. We model cell rearrangement events as
 384 occurring intermittently and randomly in a discrete spatial linear structure. We modeled
 385 the intermittency of cell rearrangement events by a jump process and analyzed the model
 386 while maintaining the discreteness of the spatial structure by considering the time evolution
 387 of the power spectrum. In our framework, the stochastic and intermittent effects of cell
 388 rearrangement were approximated by the deterministic effects on the power spectrum. Ac-
 389 cordingly, the instabilities of the pattern dynamics were analyzed by solving the maximum
 390 eigenvalue problem of the resultant systems (23) and (39).

391 Our model predicts that an increase in the frequency of cell rearrangement events will
 392 result in a more homogeneous pattern. It has been observed that endothelial cells within the
 393 retinal vasculature manifest a one-dimensional configuration, Delta-Notch pattern formation
 394 [8, 13, 14], with reported occurrences of both cell mixing and proliferation [23, 24, 32].
 395 The expression pattern of Delta-like ligand 4 (Dll4) mRNA is alternating in arteries and

396 homogeneous in veins (Fig. S12(A)). [8, 13, 14]. Our preliminary experiments indicated
397 that endothelial cell motility and proliferation rates are higher in veins than in arteries
398 (Supplementary Text B and Figure S12 [28]). This relationship has also been reported
399 in the developing zebrafish vasculature [33, 34]. Our theoretical predictions regarding the
400 relationship between the frequency of cell rearrangement events and expression patterns are
401 consistent with these experimental findings.

402 In this study, we assumed that the daughter cells inherit the same activity of Delta and
403 Notch in the cell proliferation model. However, if we adopt an asymmetric inheritance rule,
404 we obtain different pattern dynamics. Figure S13 [28] shows how the magnitude of the
405 perturbation to the expression in daughter cells caused by asymmetric cell division affects
406 heterogeneity in the cell proliferation model (7). Although the steady value of $H(t)$ decreases
407 with q as in the symmetric inheritance rule case, the time required to establish the pattern
408 decreases and the pattern maintains a certain degree of heterogeneity even for large q , and
409 does not converge to the homogeneous steady state (Figs. S13(B) and S13(C)). It should be
410 noted, however, that the results exhibited in the symmetric inheritance rule are robust if
411 the perturbation is small enough in the asymmetric inheritance rule (Fig. S13(D)).

412 Our analysis can be applied to a wide range of pattern formation mechanisms. For exam-
413 ple, a Delta-Notch interaction model that includes cis-interaction, which is the inhibition of
414 Notch activity by Delta activity, is proposed by Sprinzak *et al* [3]. This model (S47) consists
415 of three variables and has different interaction terms when compared to the Collier model
416 (1). We find that cell rearrangement events also inhibit salt and pepper pattern formation
417 in the Sprinzak model, and our analysis yields expressions for the balanced frequencies p^*
418 and q^* that are consistent with the numerical results (Supplementary text C and Fig. S14
419 [28]). To determine the stability of the homogeneous steady state, our method is effective
420 regardless of the details of model, such as the number of variables and the interaction terms,
421 and could be applied to the models including the effect of other ligands in the Delta-Notch
422 system, such as Delta-Notch-Jagged system [35].

423 In addition, phase synchronization phenomena in coupled agent-based models can be in-
424 vestigated by our analysis. Uriu *et al.* [36] showed that the exchange of positions in a coupled
425 phase oscillator system in a one-dimensional array promoted phase synchronization, and the
426 relaxation time is consistent with the mean-field approximation if the exchange frequency is
427 sufficiently large. This phase synchronization model is similar to the model we used, in the

428 sense that interactions between neighboring cells are affected by positional perturbations,
 429 suggesting we can also capture this phenomenon by interpreting phase synchronization as
 430 convergence to a homogeneous steady state of the pattern composed of the agents' phase
 431 state. We can generalize our method by replacing the effects of flip and proliferation by a
 432 linear operator acting on the power spectrum.

433 **ACKNOWLEDGEMENTS**

434 The authors thank Professor Koichi Nishiyama (Kumamoto University), Professor Shin-
 435 Ichiro Ei (Hokkaido University), Dr. Yoshitaro Tanaka (Future University Hakodate), and
 436 Dr. Kei Sugihara (Kyushu University) for helpful discussions. This work has been financially
 437 supported by JST CREST (JPMJCR14W4 to TM), JSPS KAKENHI (JP18K06260 to HT-
 438 I), and TOBITATE! Study Abroad Initiative and Young Ambassador Program (to TO).

439 **Appendix A: Dispersion-relation of the Collier model**

440 To derive the necessary and sufficient conditions for pattern formation, we performed a
 441 linear stability analysis of the Collier model (1).

442 The homogeneous steady state (D^0, N^0) in the Collier model (1) with periodic boundary
 443 conditions is given by:

$$D^0 = \frac{1}{1 + \beta(N^0)^h} \quad (\text{A1})$$

$$N^0 = \frac{2rD^0}{1 + 2rD^0}. \quad (\text{A2})$$

444 By setting $D_x = D^0 + d_x, N_x = N^0 + n_x$, where $|d_x| \ll 1, |n_x| \ll 1$, the Collier model (1)
 445 can be linearized to obtain:

$$\begin{aligned} \frac{d}{dt}d_x &= -ad_x - bn_x \\ \frac{d}{dt}n_x &= -dn_x + \alpha(d_{x-1} + d_{x+1}), \end{aligned} \quad (\text{A3})$$

446 where $a = v$, $b = (\beta hv(N^0)^{h-1}) / (1 + \beta(N^0)^h)^2$, $d = 1$, $\alpha = r / (1 + 2rD^0)^2$.

447 To examine the stability of the homogeneous steady state in the Collier model (1), we

448 consider a discrete Fourier transformation of d_x, n_x as below:

$$\begin{aligned}\delta_k(t) &= \frac{1}{\sqrt{n}} \sum_{x=1}^n d_x(t) e^{i2\pi kx/n} \\ \nu_k(t) &= \frac{1}{\sqrt{n}} \sum_{x=1}^n n_x(t) e^{i2\pi kx/n},\end{aligned}\tag{A4}$$

449 where,

$$\begin{aligned}d_x(t) &= \frac{1}{\sqrt{n}} \sum_{k=0}^{n-1} \delta_k(t) e^{-i2\pi kx/n} \\ n_x(t) &= \frac{1}{\sqrt{n}} \sum_{k=0}^{n-1} \nu_k(t) e^{-i2\pi kx/n}.\end{aligned}\tag{A5}$$

450 Here, k is the wavenumber and takes integer values from 0 to $n - 1$, while $\delta_k(t)$ and $\nu_k(t)$
451 are the Fourier coefficients that take complex values.

452 Substituting (A5) into (A3), we obtain a system of ordinary differential equations for the
453 coefficients δ_k and ν_k as below:

$$\frac{d}{dt} \begin{pmatrix} \delta_k(t) \\ \nu_k(t) \end{pmatrix} = M_k \begin{pmatrix} \delta_k(t) \\ \nu_k(t) \end{pmatrix},\tag{A6}$$

454 where

$$M_k = \begin{pmatrix} -a & -b \\ 2\alpha \cos(2\pi k/n) & -d \end{pmatrix}.\tag{A7}$$

455 Setting

$$\begin{pmatrix} \delta_k(t) \\ \nu_k(t) \end{pmatrix} = \begin{pmatrix} \delta_k(0) \\ \nu_k(0) \end{pmatrix} e^{\lambda_k t},\tag{A8}$$

456 we find that λ_k is an eigenvalue of M_k , and the solution is dominated by the larger eigenvalue
457 of the Jacobian matrix M_k (if both eigenvalues are real). Therefore, whether the components
458 δ_k, ν_k grow or decay is determined by the sign of λ_k , where:

$$\lambda_k = \frac{-(a+d) + \sqrt{(a+d)^2 - 4(ad + 2b\alpha \cos(2\pi k/n))}}{2}.\tag{A9}$$

459 Note that if λ_k is complex, then the real part of λ_k is negative and so the perturbation
460 decays with time. In the Collier model (1), λ_k in (A9) takes its largest value at $k = n/2$ and
461 negative values in the long-wavelength region (Fig. S1). As a result, $|\delta_k|$ exponentially
462 grow if k is near $n/2$ and attenuate in the other region. It is correspond to the salt and

463 pepper pattern, and the necessary and sufficient condition for pattern formation is obtained
 464 as below:

$$\lambda_{\max} = \frac{-(a+d) + \sqrt{(a+d)^2 - 4(ad - 2b\alpha)}}{2} > 0. \quad (\text{A10})$$

465 From (A1) and (A2), we have that,

$$\beta(N^0)^{h+1} = -(2r+1)N^0 + 2r. \quad (\text{A11})$$

466 Thus,

$$b = \frac{hv(2r - (2r+1)N^0)}{4r^2(1 - N^0)^2} \quad (\text{A12})$$

$$\alpha = (1 - N^0)^2 r, \quad (\text{A13})$$

467 and

$$2b\alpha = hv \left(1 - N^0 - \frac{N^0}{2r} \right). \quad (\text{A14})$$

468 Since $ad = v$ and $0 < N^0 < 1$ from (A2), $ad > 2b\alpha$ if $h \leq 1$, so that the inequality (A10)
 469 does not hold. Hence a necessary condition for (A10) to hold is $h > 1$.

470 **Appendix B: Derivation of the time evolution equation for the power spectrum**

471 **(21)**

472 From equation (20), the value of $\delta_k(t+dt)$ is given by:

$$\delta_k(t+dt) = \delta_k(t) + \lambda_k \delta_k(t) dt + \sum_{j=1}^n \sum_{l=0}^{n-1} \{C^j - I\}_{k+1, l+1} \delta_l(t) dL_t^{p,j}. \quad (\text{B1})$$

473 The value of the power spectrum $P_k(t+dt) = |\delta_k(t+dt)|^2$ is obtained by multiplying $\delta_k(t+dt)$
 474 in (B1) by its complex conjugate $\bar{\delta}_k(t+dt)$ as below:

$$\begin{aligned} |\delta_k(t+dt)|^2 &= |\delta_k(t)|^2 + \lambda_k |\delta_k(t)|^2 dt + \bar{\lambda}_k |\delta_k(t)|^2 dt \\ &+ \sum_{j=1}^n \left[\left(\bar{\delta}_k(t) \sum_{l=0}^{n-1} \{C^j - I\}_{k+1, l+1} \delta_l(t) + \delta_k(t) \sum_{l=0}^{n-1} \{\bar{C}^j - I\}_{k+1, l+1} \bar{\delta}_l(t) \right) \right. \\ &\quad \left. + \left(\sum_{l=0}^{n-1} \{C^j - I\}_{k+1, l+1} \delta_l(t) \right) \left(\sum_{l=0}^{n-1} \{\bar{C}^j - I\}_{k+1, l+1} \bar{\delta}_l(t) \right) \right] dL_t^{p,j} \\ &+ O(dL_t^{p,j} dt) + O(dt^2). \end{aligned} \quad (\text{B2})$$

475 Here we used the result:

$$(dL_t^{p,j})(dL_t^{p,\xi}) = \begin{cases} 0 & \text{if } j \neq \xi \\ dL_t^{p,j} & \text{if } j = \xi. \end{cases} \quad (\text{B3})$$

476 By denoting $a_k^j = \sum_{l=0}^{n-1} \{C^j\}_{k+1,l+1} \delta_l$, we obtain:

$$\sum_{l=0}^{n-1} \{C^j - I\}_{k+1,l+1} \delta_l(t) = a_k^j(t) - \delta_k(t). \quad (\text{B4})$$

477 Substituting (B4) into (B2), we obtain:

$$\begin{aligned} |\delta_k(t+dt)|^2 &= |\delta_k(t)|^2 + 2\text{Re}[\lambda_k] |\delta_k(t)|^2 dt + \sum_{j=1}^n [|a_k^j(t)|^2 - |\delta_k(t)|^2] dL_t^{p,j} \\ &= |\delta_k(t)|^2 + 2\text{Re}[\lambda_k] |\delta_k(t)|^2 dt + \sum_{j=1}^n \left[\left| \sum_{l=0}^{n-1} \{C^j\}_{k+1,l+1} \delta_l(t) \right|^2 - |\delta_k(t)|^2 \right] dL_t^{p,j}. \end{aligned} \quad (\text{B5})$$

478 The third term on the right-hand side of (B5) is the effect of the cell flip on the power
479 spectrum for the flip position j . Based on the symmetry of the cell position j in the system
480 (5), we assume that the third term on the right-hand side of (B5) is approximated by
481 replacing the effect of each flip event with \mathcal{W}_k , which is the averaged effect for the flip
482 position j as below:

$$\sum_{j=1}^n \left[\left| \sum_{l=0}^{n-1} \{C^j\}_{k+1,l+1} \delta_l(t) \right|^2 - |\delta_k(t)|^2 \right] dL_t^{p,j} \simeq \sum_{j=1}^n \mathcal{W}_k dL_t^{p,j} = \mathcal{W}_k dL_t^{pn}, \quad (\text{B6})$$

483 where,

$$\begin{aligned} \mathcal{W}_k &= \frac{1}{n} \sum_{j=1}^n \left[\left| \sum_{l=0}^{n-1} \{C^j\}_{k+1,l+1} \delta_l(t) \right|^2 - |\delta_k(t)|^2 \right] \\ &= \frac{1}{n} \sum_{j=1}^n \left[\left| \sum_{l=0}^{n-1} \{C^j\}_{k+1,l+1} \delta_l(t) \right|^2 \right] - |\delta_k(t)|^2 \end{aligned} \quad (\text{B7})$$

484 Here, we used $\sum_{j=1}^n dL_t^{p,j} = dL_t^{pn}$ and note that

$$\frac{1}{n} \sum_{j=1}^n \left[\left| \sum_{l=0}^{n-1} \{C^j\}_{k+1,l+1} \delta_l(t) \right|^2 \right] = \frac{1}{n} \sum_{m=0}^{n-1} \sum_{l=0}^{n-1} \left[\delta_l \overline{\delta_m} \left(\sum_{j=1}^n \{C^j\}_{k+1,l+1} \overline{\{C^j\}_{k+1,m+1}} \right) \right]. \quad (\text{B8})$$

485 From (17), the components of the matrix C^j are given as below:

$$\{C^j\}_{k,l} = \begin{cases} -\frac{4}{n} \sin \frac{\pi(l-1)}{n} \sin \frac{\pi(k-1)}{n} e^{\frac{i\pi(2j-1)(k-l)}{n}} & \text{if } k \neq l \\ 1 - \frac{4}{n} \sin^2 \frac{\pi(k-1)}{n} & \text{if } k = l, \end{cases} \quad (\text{B9})$$

486 SO,

$$\sum_{j=1}^n \{C^j\}_{k+1,l+1} \overline{\{C^j\}_{k+1,m+1}} = \begin{cases} 0 & \text{if } l \neq m \\ \frac{16}{n} \sin^2 \frac{\pi k}{n} \sin^2 \frac{\pi l}{n} & \text{if } l = m \text{ and } k \neq m \\ n \left(1 - \frac{4}{n} \sin^2 \frac{\pi k}{n}\right)^2 & \text{if } k = l = m. \end{cases} \quad (\text{B10})$$

487 Here we used

$$\sum_{j=1}^n e^{i\pi(2j-1)(l-m)/n} = \begin{cases} 0 & \text{if } l \neq m \\ n & \text{if } l = m. \end{cases} \quad (\text{B11})$$

488 Therefore, from (B8) and (B10), we obtain:

$$\begin{aligned} & \frac{1}{n} \sum_{j=1}^n \left[\left| \sum_{l=0}^{n-1} \{C^j\}_{k+1,l+1} \delta_l(t) \right|^2 \right] \\ &= \frac{1}{n} \sum_{\substack{l=0 \\ l \neq k}}^{n-1} \left[|\delta_l(t)|^2 \frac{16}{n} \sin^2 \frac{\pi k}{n} \sin^2 \frac{\pi l}{n} \right] + |\delta_k(t)|^2 \left(1 - \frac{8}{n} \sin^2 \frac{\pi k}{n} + \frac{16}{n^2} \sin^4 \frac{\pi k}{n} \right) \\ &= \sum_{l=0}^{n-1} \left[\left(\frac{4}{n} \sin \frac{\pi k}{n} \sin \frac{\pi l}{n} \right)^2 |\delta_l(t)|^2 \right] + \left(1 - \frac{8}{n} \sin^2 \frac{\pi k}{n} \right) |\delta_k(t)|^2. \end{aligned} \quad (\text{B12})$$

489 By replacing the third term on the right-hand side of (B5) by the averaged effect (B6) and
490 substituting (B7) and (B12), we obtain:

$$\begin{aligned} |\delta_k(t+dt)|^2 &\simeq |\delta_k(t)|^2 + 2\text{Re}[\lambda_k] |\delta_k(t)|^2 dt + \frac{1}{n} \sum_{j=1}^n \left[\left| \sum_{l=0}^{n-1} \{C^j\}_{k+1,l+1} \delta_l(t) \right|^2 - |\delta_k(t)|^2 \right] dL_t^{pn} \\ &= |\delta_k(t)|^2 + 2\text{Re}[\lambda_k] |\delta_k(t)|^2 dt \\ &\quad + \left(\sum_{l=0}^{n-1} \left[\left(\frac{4}{n} \sin \frac{\pi k}{n} \sin \frac{\pi l}{n} \right)^2 |\delta_l(t)|^2 \right] - \frac{8}{n} \sin^2 \frac{\pi k}{n} |\delta_k(t)|^2 \right) dL_t^{pn}. \end{aligned} \quad (\text{B13})$$

491 Therefore, the time evolution of the power spectrum can be represented more concisely in
492 the form:

$$d\mathbf{P} = 2\text{Re}[\Lambda] \mathbf{P} dt + W \mathbf{P} dL_t^{pn}, \quad (\text{B14})$$

493 where Λ is given in (15), $\mathbf{P} = (|\delta_0(t)|^2, |\delta_1(t)|^2, \dots, |\delta_k(t)|^2, \dots, |\delta_{n-1}(t)|^2)^\top$ and

$$\{W\}_{l,m} = \begin{cases} -\frac{8}{n} \sin^2 \frac{\pi(l-1)}{n} + \left(\frac{4}{n} \sin^2 \frac{\pi(l-1)}{n}\right)^2 & (l = m) \\ \left(\frac{4}{n} \sin \frac{\pi(l-1)}{n} \sin \frac{\pi(m-1)}{n}\right)^2 & (\text{otherwise}). \end{cases} \quad (\text{B15})$$

494 **Appendix C: Derivation of the time evolution of the power spectrum (36)**

495 From equation (31), the components of the matrix \hat{C}^j are given as below:

$$\{\hat{C}^j\}_{k,l} = \begin{cases} \sqrt{(n+1)/n} & (\text{if } k = l = 1) \\ -\frac{1}{\sqrt{n(n+1)}} \frac{\sin\left(\frac{\pi(l-1)}{n}\right)}{\sin\left(\frac{\pi(k-1)}{n+1} - \frac{\pi(l-1)}{n}\right)} e^{i\pi\left(\frac{(2j-1)(k-1)}{n+1} - \frac{2(j-1)(l-1)}{n}\right)} & (\text{otherwise}) \end{cases}. \quad (\text{C1})$$

496 The power spectrum after proliferation of cell j is obtained from the Fourier coefficient δ_k
497 before proliferation as below:

$$\begin{aligned} |\delta_{k-1}|_{\text{after}}^{2j} &= \left(\sum_{l=1}^n \{\hat{C}^j\}_{k,l} \delta_{l-1} \right) \left(\sum_{m=1}^n \{\bar{C}^j\}_{k,m} \bar{\delta}_{m-1} \right) \\ &= \sum_{m=1}^n \sum_{l=1}^n \left[\{\hat{C}^j\}_{k,l} \{\bar{C}^j\}_{k,m} \delta_{l-1} \bar{\delta}_{m-1} \right]. \end{aligned} \quad (\text{C2})$$

498 As in the cell mixing model, the time evolution of the power spectrum is approximated
499 by replacing the effect of each proliferation event with an average effect. Considering the
500 average effect on the power spectrum, we calculate the average of $|\delta_k|_{\text{after}}^{2j}$ over j :

$$\begin{aligned} \frac{1}{n} \sum_{j=1}^n |\delta_{k-1}|_{\text{after}}^{2j} &= \frac{1}{n} \sum_{j=1}^n \sum_{m=1}^n \sum_{l=1}^n \left[\{\hat{C}^j\}_{k,l} \{\bar{C}^j\}_{k,m} \delta_{l-1} \bar{\delta}_{m-1} \right] \\ &= \frac{1}{n} \sum_{m=1}^n \sum_{l=1}^n \delta_{l-1} \bar{\delta}_{m-1} \left[\sum_{j=1}^n \{\hat{C}^j\}_{k,l} \{\bar{C}^j\}_{k,m} \right], \end{aligned} \quad (\text{C3})$$

501 and

$$\sum_{j=1}^n \{\hat{C}^j\}_{k,l} \{\bar{C}^j\}_{k,m} = \begin{cases} 0 & \text{if } l \neq m \\ \frac{1}{(n+1)} \frac{\sin^2 \frac{\pi(l-1)}{n}}{\sin^2 \left(\frac{\pi(k-1)}{n+1} - \frac{\pi(l-1)}{n} \right)} & \text{if } l = m \text{ and } l \neq 1 \\ (n+1) & \text{if } k = l = m = 1. \end{cases} \quad (\text{C4})$$

502 Here we used the fact that

$$\sum_{j=1}^n e^{i2\pi(j-1)(l-m)/n} = \begin{cases} 0 & \text{if } l \neq m \\ n & \text{if } l = m. \end{cases} \quad (\text{C5})$$

503 Hence,

$$\frac{1}{n} \sum_{j=1}^n |\delta_{k-1}|^2_{\text{after}} = \begin{cases} \sum_{l=1}^n \frac{1}{n(n+1)} \frac{\sin^2\left(\frac{\pi(l-1)}{n}\right)}{\sin^2\left(\frac{\pi(k-1)}{n+1} - \frac{\pi(l-1)}{n}\right)} |\delta_{l-1}|^2 & \text{if } k \neq 1 \\ \frac{n+1}{n} |\delta_0|^2 + \frac{1}{n(n+1)} \sum_{l=2}^n |\delta_{l-1}|^2 & \text{if } k = 1. \end{cases} \quad (\text{C6})$$

504 Therefore, the effect of a single proliferation event on the power spectrum is represented by
505 the matrix S in (34).

506 Since the Delta expression D_x are real values, $P_k = P_{n-k}$ hold. Because of this symmetry,
507 \mathbf{P}_n is represented by the superposition of cosine waves:

$$\mathbf{P}_n = \sum_{k=0}^{n-1} e_k \mathbf{z}_k^n, \quad (\text{C7})$$

$$\mathbf{z}_k^n = \left(1, \cos \frac{2\pi k}{n}, \cos \frac{4\pi k}{n}, \dots, \cos \frac{2(n-1)\pi k}{n} \right)^\top. \quad (\text{C8})$$

508 Here, e_k are the coefficients of superposition. From the orthogonality of the trigonometric
509 function, we obtain:

$$\mathbf{e} = Z \mathbf{P}_n, \quad (\text{C9})$$

510 where $\mathbf{e} = (e_0, e_1, \dots, e_{n-1})^\top$ and Z is a square $n \times n$ matrix such that:

$$\{Z\}_{l,m} = \cos \frac{2\pi(l-1)(m-1)}{n}. \quad (\text{C10})$$

511 From the symmetry of \mathbf{P}_n , we can also obtain e_k as a discrete Fourier transform of \mathbf{P}_n . As
512 the discrete Fourier transform of the power spectrum is the auto-correlation function (from
513 the Wiener-Khinchin theorem), e_k corresponds to the averaged auto-correlation function of
514 D_x .

515 $S\mathbf{P}_n$ is also represented by the superposition of cosine waves with different coefficients
516 \hat{e}_k :

$$S\mathbf{P}_n = \sum_{k=0}^n \hat{e}_k \mathbf{z}_k^{n+1}. \quad (\text{C11})$$

517 Therefore, the power spectra \mathbf{P}_n and $S\mathbf{P}_n$ can be regarded as the sampled values of the
518 function $P(\theta)$ and $P(\theta)_{\text{after}}$, respectively:

$$P(\theta) = \sum_{k=0}^{n-1} e_k \cos kx \quad (\text{C12})$$

$$P(\theta)_{\text{after}} = \sum_{k=0}^n \hat{e}_k \cos kx. \quad (\text{C13})$$

519 Then the matrix S can be regarded as a map that transfers the coefficients of superposition
 520 e_k to \hat{e}_k .

521 The vector $2\text{Re}[\Lambda]\mathbf{P}_n$ is also regarded as the sampled values of the function $2\lambda(\theta)P(\theta)$,
 522 where

$$\lambda(\theta) = \text{Re} \left[\frac{-(a+d) + \sqrt{(a+d)^2 - 4(ad + 2b\alpha \cos \theta)}}{2} \right]. \quad (\text{C14})$$

523 Therefore, the stability of the power spectrum vector \mathbf{P}_n can be examined by approximating
 524 S with a square matrix Σ such that $\Sigma\mathbf{P}_n$ share the same coefficients of the superposition
 525 with $S\mathbf{P}_n$.

526 We write

$$S = \frac{1}{n} \hat{Z} Q Z, \quad (\text{C15})$$

527 where \hat{Z} is a square $(n+1) \times (n+1)$ matrix and Q is an $(n+1) \times n$ matrix whose components
 528 are, respectively,

$$\{\hat{Z}\}_{l,m} = \cos \frac{2\pi(l-1)(m-1)}{n+1}, \quad (\text{C16})$$

529 and

$$\{Q\}_{l,m} = \begin{cases} (n+2-l)/(n+1) & (\text{if } l=m) \\ (l-1)/(n+1) & (\text{if } l+1=m \text{ and } l \geq 2) \\ 1/(n+1) & (\text{if } l=n \text{ and } m=1) \\ 0 & (\text{otherwise}) \end{cases}. \quad (\text{C17})$$

530 Therefore, the coefficients \hat{e}_k are determined by e_k as follows:

$$\begin{aligned} \hat{e}_0 &= e_0 \\ \hat{e}_k &= \frac{n+1-k}{n+1} e_k + \frac{k}{n+1} e_{k-1} \quad (1 \leq k \leq n-1) \\ \hat{e}_n &= \frac{n}{n+1} e_{n-1} + \frac{1}{n+1} e_0. \end{aligned} \quad (\text{C18})$$

531 This relationship is derived from the formulae in Supplementary text B [28].

532 When n is even, we define an $n \times n$ square matrix \hat{Q} by removing the $(n/2 + 1)$ -th row
 533 of the matrix Q , and then define an $n \times n$ square matrix Σ such that:

$$\Sigma = Z \hat{Q} Z. \quad (\text{C19})$$

534 Here,

$$\begin{aligned} \{\Sigma\}_{l,m} &= \frac{2}{n} \sum_{k=2}^{n/2} \cos \frac{2\pi(m-1)(k-1)}{n} \left[\frac{k-1}{n+1} \cos \frac{2\pi(l-1)(k-2)}{n} + \left(1 - \frac{k-1}{n+1}\right) \cos \frac{2\pi(l-1)(k-1)}{n} \right] \\ &\quad + \frac{1}{n} \left(1 + (-1)^{m+l-2} \left(1 - \frac{n}{n+1} \sin^2 \frac{\pi(l-1)}{n} \right) \right). \end{aligned} \quad (\text{C20})$$

535 The n dimensional vector $\Sigma \mathbf{P}_n$ is represented as the superposition of the cosine waves:

$$\Sigma \mathbf{P}_n = \sum_{k=0}^{n/2} \hat{e}_k \mathbf{z}_k^n + \sum_{k=n/2+1}^{n-1} \hat{e}_{k+1} \mathbf{z}_k^n. \quad (\text{C21})$$

536 Since $z_k^n = z_{n-k}^n$ holds and n is even, equation (C11) can be simplified:

$$S \mathbf{P}_n = \sum_{k=0}^{n/2} \tilde{e}_k \mathbf{z}_k^{n+1} \quad (\text{C22})$$

$$\tilde{e}_k = \begin{cases} \hat{e}_k & (\text{if } k=0) \\ \hat{e}_k + \hat{e}_{n-k} & (\text{otherwise}) \end{cases}. \quad (\text{C23})$$

537 Equation (C21) can also be simplified:

$$\Sigma \mathbf{P}_n = \left(\sum_{k=0}^{n/2-1} \tilde{e}_k \mathbf{z}_k^n \right) + \hat{e}_{n/2} \mathbf{z}_{n/2}^n. \quad (\text{C24})$$

538 When n is odd, we define an $n \times n$ square matrix \hat{Q} by removing the $((n+3)/2)$ -th row
539 of the matrix Q , and define an $n \times n$ square matrix Σ such that:

$$\Sigma = Z \hat{Q} Z. \quad (\text{C25})$$

540 Here,

$$\begin{aligned} \{\Sigma\}_{l,m} &= \frac{2}{n} \sum_{k=2}^{(n+1)/2} \cos \frac{2\pi(m-1)(k-1)}{n} \left[\frac{k-1}{n+1} \cos \frac{2\pi(l-1)(k-2)}{n} + \left(1 - \frac{k-1}{n+1}\right) \cos \frac{2\pi(l-1)(k-1)}{n} \right] \\ &\quad + \frac{1}{n}. \end{aligned} \quad (\text{C26})$$

541 The n dimensional vector $\Sigma \mathbf{P}_n$ is represented as the superposition of the cosine waves:

$$\Sigma \mathbf{P}_n = \sum_{k=0}^{(n-1)/2} \hat{e}_k \mathbf{z}_k^n + \sum_{k=(n+1)/2}^{n-1} \hat{e}_{k+1} \mathbf{z}_k^n. \quad (\text{C27})$$

542 Since n is odd, equation (C11) can be simplified:

$$S\mathbf{P}_n = \sum_{k=0}^{(n+1)/2} \tilde{e}_k \mathbf{z}_k^{n+1} \quad (\text{C28})$$

$$\tilde{e}_k = \begin{cases} \hat{e}_k & (\text{if } k = 0 \text{ or } (n+1)/2) \\ \hat{e}_k + \hat{e}_{n-k} & (\text{otherwise}) \end{cases}. \quad (\text{C29})$$

543 Equation (C27) can also be simplified:

$$\Sigma\mathbf{P}_n = \sum_{k=0}^{(n-1)/2} \tilde{e}_k \mathbf{z}_k^n. \quad (\text{C30})$$

544 Comparing (C24) with (C22) and (C30) with (C28), $\Sigma\mathbf{P}_n$ and $S\mathbf{P}_n$ can be represented
 545 by the same cosine wave superposition except for that of the shortest wavelength ($\tilde{e}_{n/2}$ when
 546 n is even, $\tilde{e}_{(n+1)/2}$ when n is odd).

547 The shortest wavelength component of the superposition $\tilde{e}_{n/2}$ or $\tilde{e}_{(n+1)/2}$ corresponds to
 548 the long-range correlation of the Delta expression pattern \mathbf{D}_n . Since the Delta-Notch inter-
 549 action and cell proliferation locally affects the pattern, we expect the long-range correlation
 550 to be small. Thus, the contribution of the shortest wavelength component of the cosine wave
 551 superposition alone to the spectral structure of the power spectrum would be small when
 552 n is sufficiently large. Therefore, Σ is a square matrix that approximates S , in the sense
 553 that it preserves the spectral structure of the power spectrum. Based on this assumption,
 554 we can analyze equation (34) in the same way as in the cell mixing model by replacing S
 555 with Σ , and find that it gives the results that agree with the numerical results of the cell
 556 proliferation model (7) (Figs. 4(D) and 4(F)).

- 557 [1] O. L. Mohr, *Genetics* **4**, 275 (1919).
 558 [2] J. R. Collier, N. A. M. Monk, P. K. Maini, and J. H. Lewis, *J. Theor. Biol.* **183**, 429 (1996).
 559 [3] D. Sprinzak, A. Lakhanpal, L. LeBon, L. A. Santat, M. E. Fontes, G. A. Anderson, J. Garcia-
 560 Ojalvo, and M. B. Elowitz, *Nature* **465**, 86 (2010).
 561 [4] F. Vilas-Boas, R. Fior, J. R. Swedlow, K. G. Storey, and D. Henrique, *BMC Biol.* **9**, 58
 562 (2011).
 563 [5] O. Shaya and D. Sprinzak, *Curr. Opin. Genet. Dev.* **21**, 732 (2011).

- 564 [6] M. Matsuda, M. Koga, E. Nishida, and M. Ebisuya, *Sci. Signal* **5**, ra31 (2012).
- 565 [7] K. Uriu and L. G. Morelli, *Dev. Growth Differ.* **59**, 351 (2017).
- 566 [8] A. M. Herman, A. M. Rhyner, W. P. Devine, S. P. Marrelli, B. G. Bruneau, and J. D. Wythe,
567 *Biol. Open* **7**, bio026799 (2018).
- 568 [9] M. E. Pitulescu, I. Schmidt, B. D. Giaimo, T. Antoine, F. Berkenfeld, F. Ferrante, H. Park,
569 M. Ehling, D. Biljes, S. F. Rocha, U. H. Langen, M. Stehling, T. Nagasawa, N. Ferrara,
570 T. Borggreffe, and R. H. Adams, *Nat. Cell Biol.* **19**, 915 (2017).
- 571 [10] M. Eddison, I. L. Roux, and J. Lewis, *Proc. Natl. Acad. Sci. U.S.A.* **97**, 11692 (2000).
- 572 [11] E. Chrysostomou, J. E. Gale, and N. Daudet, *Development* **139**, 3764 (2012).
- 573 [12] J. Neves, G. Abelló, J. Petrovic, and F. Giraldez, *Dev. Growth Differ.* **55**, 96 (2013).
- 574 [13] S. Claxton and M. Fruttiger, *Gene Expr. Patterns* **5**, 123 (2004).
- 575 [14] J. J. Hofmann and M. L. Iruela-Arispe, *Gene Expr. Patterns* **7**, 461 (2006).
- 576 [15] S. S. Hasan, R. Tsaryk, M. Lange, L. Wisniewski, J. C. Moore, N. D. Lawson, K. Woj-
577 ciechowska, H. Schnittler, and A. F. Siekmann, *Nat. Cell Biol.* **19**, 928 (2017).
- 578 [16] M. Cohen, B. Baum, and M. Miodownik, *J. R. Soc. Interface* **8**, 787 (2010).
- 579 [17] M. B. Elowitz, A. J. Levine, E. D. Siggia, and P. S. Swain, *Science* **297**, 1183 (2002).
- 580 [18] D. A. Charlebois, N. Abdennur, and M. Kaern, *Phys. Rev. Lett.* **107**, 218101 (2011).
- 581 [19] T. Rudge and K. Burrage, *Bull. Math. Biol.* **70**, 971 (2008).
- 582 [20] A. I. Reppas, G. Lolas, A. Deutsch, and H. Hatzikirou, *ACM Trans. Model. Comput. Simul.*
583 **26**, 19 (2016).
- 584 [21] M. Noguchi, K. Sumiyama, and M. Morimoto, *Cell Rep.* **13**, 2679 (2015).
- 585 [22] P.-N. Tsao, C. Matsuoka, S.-C. Wei, A. Sato, S. Sato, K. Hasegawa, H.-k. Chen, T.-Y. Ling,
586 M. Mori, W. V. Cardoso, and M. Morimoto, *Proc. Natl. Acad. Sci. U.S.A.* **113**, 8242 (2016).
- 587 [23] S. Arima, K. Nishiyama, T. Ko, Y. Arima, Y. Hakozaiki, K. Sugihara, H. Koseki, Y. Uchijima,
588 Y. Kurihara, and H. Kurihara, *Development* **138**, 4763 (2011).
- 589 [24] W. Luo, I. Garcia-Gonzalez, M. Fernández-Chacón, V. Casquero-Garcia, M. S. Sanchez-
590 Muñoz, S. Mühleder, L. Garcia-Ortega, J. Andrade, M. Potente, and R. Bedito, *Nature*
591 **589**, 437 (2020).
- 592 [25] R. Riahi, J. Sun, S. Wang, M. Long, D. D. Zhang, and P. K. Wong, *Nat. Commun.* **6**, 6556
593 (2015).
- 594 [26] D. P. J. Germano and J. M. Osborne, *J. Theor. Biol.* **514**, 110535 (2021).

- 595 [27] D. Stepanova, H. M. Byrne, P. K. Maini, and T. Alarcón, *PLoS Comput. Biol.* **17**, e1008055
596 (2021).
- 597 [28] See Supplemental Material at [URL will be inserted by publisher] for additional information
598 and figures.
- 599 [29] P. Formosa-Jordan, Pattern formation through lateral inhibition mediated by Notch signaling,
600 Ph.D. thesis, Universitat de Barcelona (2013).
- 601 [30] H. X. Chao, R. I. Fakhreddin, H. K. Shimerov, K. M. Kedziora, R. J. Kumar, J. Perez, J. C.
602 Limas, G. D. Grant, J. G. Cook, G. P. Gupta, and J. E. Purvis, *Mol. Syst. Biol.* **15**, e8604
603 (2019).
- 604 [31] P. Formosa-Jordan and M. Ibañez, *PloS one* **9**, e95744 (2014).
- 605 [32] S. Pontes-Quero, M. Fernández-Chacón, W. Luo, F. F. Lunella, V. Casquero-Garcia, I. Garcia-
606 Gonzalez, A. Hermoso, S. F. Rocha, M. Bansal, and R. Benedito, *Nat. Commun.* **10**, 2016
607 (2019).
- 608 [33] C. Xu, S. S. Hasan, I. Schmidt, S. F. Rocha, M. E. Pitulescu, J. Bussmann, D. Meyen, E. Raz,
609 R. H. Adams, and A. F. Siekmann, *Nat. Commun.* **5**, 5758 (2014).
- 610 [34] B. Weijts, E. Gutierrez, S. K. Saikin, A. J. Ablooglu, D. Traver, A. Groisman, and
611 E. Tkachenko, *Nat. Commun.* **9**, 5314 (2018).
- 612 [35] M. K. Jolly, M. Boareto, M. Lu, J. N. Onuchic, C. Clementi, and E. Ben-Jacob, *New J. Phys.*
613 **17**, 055021 (2015).
- 614 [36] K. Uriu, S. Ares, A. C. Oates, and L. G. Morelli, *Phys. Rev. E* **87**, 032911 (2013).
- 615 [37] T. Abe, H. Kiyonari, G. Shioi, K. Inoue, K. Nakao, S. Aizawa, and T. Fujimori, *genesis* **49**,
616 579 (2011).
- 617 [38] J. M. Ogilvie, J. D. Speck, J. M. Lett, and T. T. Fleming, *J. Neurosci. Methods* **87**, 57 (1999).
- 618 [39] J. Schindelin, I. Arganda-Carreras, E. Frise, V. Kaynig, M. Longair, T. Pietzsch, S. Preibisch,
619 C. Rueden, S. Saalfeld, B. Schmid, *Nat. Methods* **9**, 676 (2012).
- 620 [40] J. Tinevez, N. Perry, J. Schindelin, G. M. Hoopes, G. D. Reynolds, E. Laplantine, S. Y.
621 Bednarek, S. L. Shorte, and K. W. Eliceiri, *Methods* **115**, 80 (2017).
- 622 [41] R. Jentzsch, *J. für die Reine und Angew. Math.* **141**, 235 (1912).
- 623 [42] X. Wang and D.-Y. Zheng, *J. Math. Anal. Appl.* **335**, 1020 (2007).
- 624 [43] W. Ejsmont and F. Lehner, *J. Comb. Theory Ser. A* **177**, 105324 (2021).

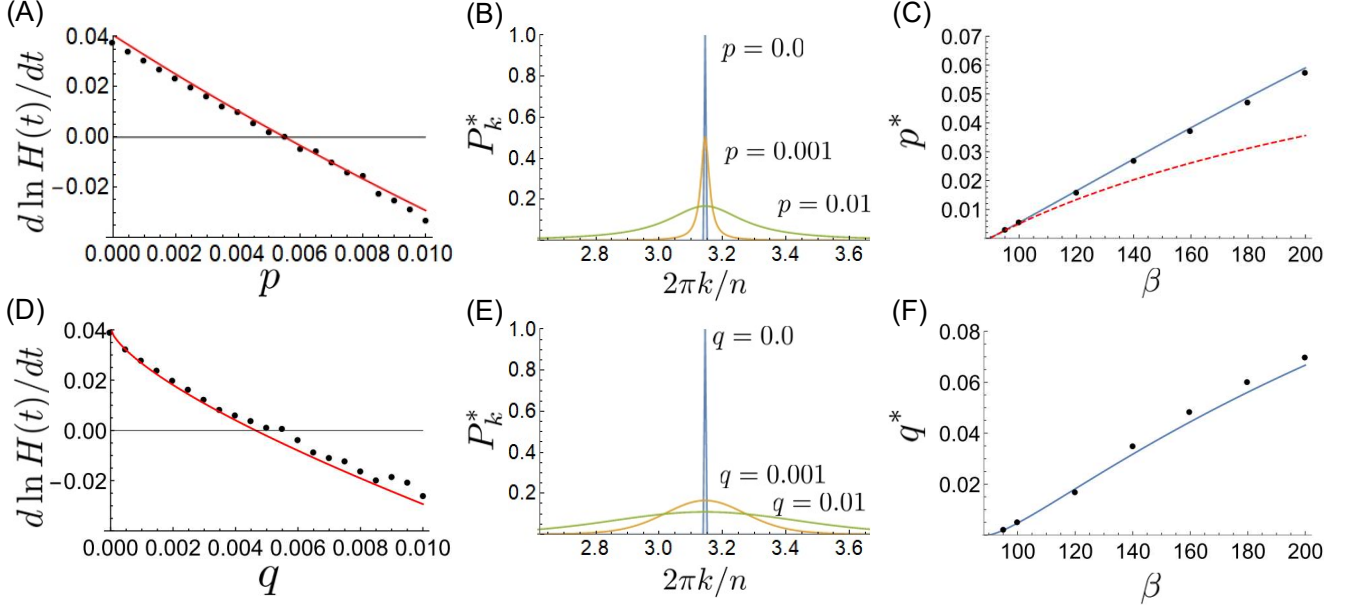


FIG. 4. Comparison between the analytical and numerical results. (A) The red line and the black dots represent the maximum eigenvalue y of the matrix Y_p in (23) and the growth rate $d \ln H(t)/dt$ estimated from Fig. S1(A) [28], respectively. (B) Normalized corresponding eigenvector \mathbf{P}^* with the maximum eigenvalue of the matrix Y_p with $n = 1000$. (C) balanced frequencies p^* plotted against the parameter β in the Collier model (1). The blue solid line represents the values of p such that the maximum eigenvalue of Y_p in (23) is 0, the red dashed line represents p^* derived from (29) and the black dots represent the values of p^* that were estimated from Fig. 3(A). (D) The red line and the black dots represent the maximum eigenvalue of the matrix J_q in (39) and the growth rate $d \ln H(t)/dt$ estimated from Fig. S1(B) [28], respectively. (E) Normalized corresponding eigenvector \mathbf{P}_k^* with the maximum eigenvalue of the matrix J_q with $n = 1000$. (F) Balanced frequencies q^* plotted against the parameter β . The blue line represents the value of q such that the maximum eigenvalue of J_q in (39) is 0, and the black dots represent the values of q^* that were estimated from Fig. 3(B), respectively. The numerically estimated growth rate $d \ln H(t)/dt$ (black dots in (A) and (D)) were calculated from the slope of the lines that were fitted to the plot of $\ln H(t)$ against t (Fig. S1 [28]). The numerically estimated balanced frequencies (black dots in (C) and (F)) were estimated as the intersection points of the plot of $\ln H^*(t)$ as a function of p and q and the plot of $\ln H^*(t) = 0$ in Fig. 3, respectively.